Available online at www.sciencedirect.com
ScienceDirect
Computerized Medical Imaging and Graphics 32 (2008) 720–727
Computerized Medical Imaging and Graphics
www.elsevier.com/locate/compmedimag

Automatic detection of diabetic retinopathy exudates from non-dilated retinal images using mathematical morphology methods

Akara Sopharak [a,*], Bunyarit Uyyanonvara [a,1], Sarah Barman [b], Thomas H. Williamson [c]

[a] *Department of Information Technology, Sirindhorn International Institute of Technology (SIIT), Thammasat University, 131 Moo 5, Tiwanont Road, Bangkadi, Muang, Pathumthani 12000, Thailand*
[b] *Faculty of Computing, Information Systems and Mathematics, Kingston University, Penrhyn Road, Kingston upon Thames, Surrey KT1 2EE, UK*
[c] *Department of Ophthalmology, St. Thomas' Hospital, London SE1 7EH, UK*

Received 23 November 2007; received in revised form 1 August 2008; accepted 26 August 2008

Abstract

Diabetic retinopathy is a complication of diabetes that is caused by changes in the blood vessels of the retina. The symptoms can blur or distort the patient's vision and are a main cause of blindness. Exudates are one of the primary signs of diabetic retinopathy. Detection of exudates by ophthalmologists normally requires pupil dilation using a chemical solution which takes time and affects patients. This paper investigates and proposes a set of optimally adjusted morphological operators to be used for exudate detection on diabetic retinopathy patients' non-dilated pupil and low-contrast images. These automatically detected exudates are validated by comparing with expert ophthalmologists' hand-drawn ground-truths. The results are successful and the sensitivity and specificity for our exudate detection is 80% and 99.5%, respectively.

Keywords: Diabetic retinopathy; Exudates; Retinal image; Non-dilated retinal images; Morphology

1. Introduction

Diabetes is the commonest cause of blindness in the working age group in the developed world. Patient's sight can be affected by diabetes which causes cataracts, glaucoma, and most importantly, damage to blood vessels inside the eye, a condition known as "diabetic retinopathy". Diabetic retinopathy is a critical eye disease which can be regarded as manifestation of diabetes on the retina. The screening of diabetic patients for the development of diabetic retinopathy can potentially reduce the risk of blindness in these patients by 50% [1–3].

Diabetic retinopathy is characterized by the development of retinal microaneurysms, haemorrhages and exudates. Microaneurysms are focal dilatations of retinal capillaries and appear as small round dark red dots. Haemorrhages occur when blood leaks from the retinal vessels. Exudates occur when lipid or fat leaks from abnormal blood vessel or aneurysms. The number of microaneurysms, haemorrhages and exudates increases as the degree of disease [4]. A number of techniques for microaneurysm and haemorrhage detection have been proposed. Sinthanayothin et al. [5] applied recursive region growing segmentation (RRGS) technique to segment vessels, microaneurysms and haemorrhages. The vessels were detected using a neural network. The remaining objects after vessels had been removed were labelled as microaneurysms and haemorrhages. Niemeijer et al. [6] proposed a method to detect candidate red lesions (microaneurysms and haemorrhages) using a pixel classification technique. Then the detected red lesion candidates were classified using a number of features and a k-nearest neighbour classifier. Usher et al. [7] used an RRGS, adaptive intensity thresholding and edge enhancement operator to extract the candidate red lesions. Candidate red lesions were classified using a neural network. However, in this paper we concentrate on exudate detection as a visible sign of diabetic retinopathy and a marker for the presence of coexistent retinal edema. If the exudates extend into the macular area, vision loss can occur.

Fluorescein angiogram images provide important information on pathologies. The most effective and accurate ways to

* Corresponding author. Tel.: +66 2501 3505; fax: +66 2501 3524.
E-mail addresses: akara@siit.tu.ac.th (A. Sopharak), bunyarit@siit.tu.ac.th (B. Uyyanonvara), s.barman@kingston.ac.uk (S. Barman), tom@retinasurgery.co.uk (T.H. Williamson).
[1] Tel.: +66 2501 3505; fax: +66 2501 3524.

0895-6111/$ – see front matter © 2008 Elsevier Ltd. All rights reserved.
doi:10.1016/j.compmedimag.2008.08.009

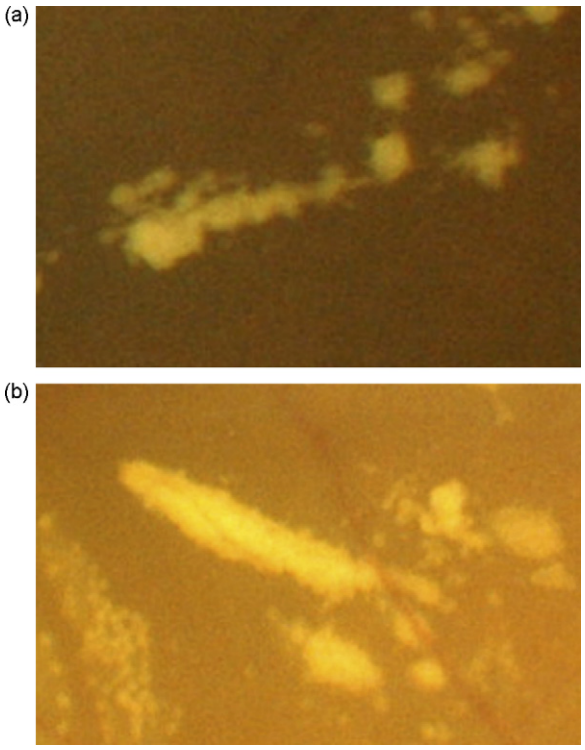

Fig. 1. (a) and (b) Retinal image containing exudates.

observe and diagnose diabetic macular edema are to investigate a fluorescein angiography. In practical terms, the decision whether to laser treat the retina does not depend significantly on the images from fluorescein angiography, it is mostly done without this investigation. The fluorescein angiograms are not suitable for an automatic screening system because there are side-effects associated with giving a patient fluorescein. The use of colour fundus images is more suitable for an automatic screening system. An automatic exudate detection system would be useful in order to detect and treat diabetic retinopathy in an early stage.

From visual inspection, exudates appear differently in a yellowish or white colour with varying sizes, shape and locations. They are often seen in either individual streaks or clusters or in large circinate structures surrounding clusters of microaneurysms. At the same time, some of them are seen in varying sizes, shape and locations as shown in Fig. 1(a) and (b).

Many techniques have been employed to the exudate detection. Gardner et al. [8] proposed an automatic detection of diabetic retinopathy using an artificial neural network. The exudates are identified from grey level images. The fundus image was analyzed using a back propagation neural network. The technique did not work well on low contrast images.

The thresholding and RRGS technique were widely used. Sinthanayothin et al. [5] reported the result of an automated detection of diabetic retinopathy on digital fundus images by RRGS algorithm where the performance was measured on 10×10 patches rather on the whole image. Usher et al. [7] detected the candidate exudates region by using a combination of RRGS and adaptive intensity thresholding. The candidate regions were extracted and used as input to a neural network. Poor quality images affected the separation result of bright and dark lesions using thresholding and exudate feature extraction using RRGS algorithm. Zheng et al. [9] detected exudates using thresholding and a region growing algorithm. The fundus photographs were taken with a non-mydriatic fundus camera and were then scanned by a flat-bed scanner.

Colour normalization and local contrast enhancement followed by fuzzy C-means clustering and neural networks were used by Osareh et al. [10]. The system works well only on Luv colour space but in the case of non-uniform illumination the detection accuracy is low. Mitra et al. [11] applied naïve Bayes classifier for diagnosis of diseases from retinal image. A system can provide a good decision support to ophthalmologist.

Much work has been performed for exudate detection based on variety of techniques. Most techniques mentioned earlier worked on dilated pupils in which the exudates and other retinal features are clearly visible. Based on experimental work reported in previous work, good quality images with larger fields are required. The retinal image of the patient must be clear enough to show retinal detail. Low quality images (non-uniform illumination, low contrast, blur or faint image) do not perform well even when enhancement processes were included. The examination time and effect on the patient could be reduced if the system can succeed on non-dilated pupils. Furthermore, many techniques required intensive computing power for training and classification.

This paper proposes an exudate detection techniques based on mathematical morphology on retinal images of non-dilated pupils that are low quality images. We based our work on this technique because it is very fast and requires lower computing power. So that the final system can be used even on a very poor computer system, such as those that may be available in rural area in developing countries where both expert ophthalmologists and high performance computers are rarely available. In addition, the location of exudates based on macular position is important information for an ophthalmologist [12,13]. They show the severity of disease, where exudates that appear closer to the macular indicate an increased severity of disease. A grid circle centred on the macular was added to provide improved diagnosis to the ophthalmologist.

2. Methods

All digital retinal images were taken from patients with non-dilated pupils using a KOWA-7 non-mydriatic retinal camera with a 45° field of view and taken at Thammasat University Hospital. The images were stored in JPEG image format files (.jpg) with lowest compression rates. The image size is 752×500 pixels at 24 bits per pixel. The overall procedure of exudate detection is demonstrated in Fig. 2.

2.1. Preprocessing

The red, green and blue (RGB) space of the original image was transformed to Hue, saturation and intensity (HSI) space because HSI colour space is more appropriate since it allows the intensity component to be separated from the other two

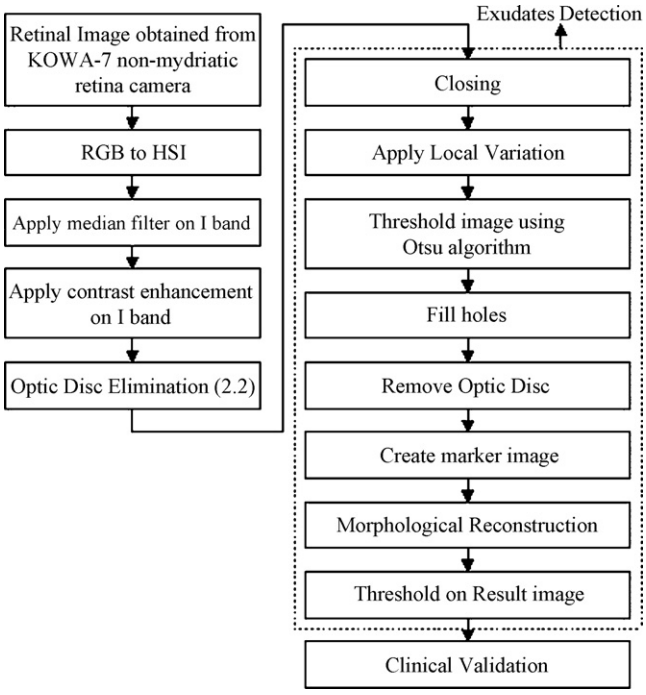

Fig. 2. Procedure of the proposed exudates detection.

colour components. A median filtering operation was then applied on I band to reduce noise before a contrast-limited adaptive histogram equalization (CLAHE) was applied for contrast enhancement [14]. CLAHE operates on small regions in the image. The contrast of each small region is enhanced with histogram equalization. After performing the equalizations, the neighbouring small regions were then combined by using bilinear interpolation.

Exudate lesions and optic disc regions normally show high intensity values in this channel and thus the contrast enhancement technique assigns them the highest intensity values [10,15].

2.2. Optic disc elimination

Exudate detection is our main purpose; however we have to remove the optic disc prior to the process because it appears with similar intensity, colour and contrast to other features on the retinal image [15–18]. The optic disc is characterized by the largest high contrast among circular shape areas. While vessels also appear with high contrast, the size of the area is much smaller. Applying a grayscale closing operator (ϕ) on the intensity channel (f_I) will help eliminate the vessels which may remain in the optic disc region. A flat disc-shaped structuring element with a fixed radius of eight (B_1) was used. Fig. 3(a) shows a result after closing operator (Eq. (1)) was applied.

$$\mathrm{OP}_1 = \phi^{(B_1)}(f_I) \tag{1}$$

where B_1 is the morphological structuring element.

The resulting image was binarized by thresholding (α_1), shown in Fig. 3(b) and the thresholded image was then used as a mask. All the pixels in the mask were inverted before they were overlaid on the original image to remove candidate bright regions. The result, OP_2, is shown in Fig. 3(c). The morphological reconstruction by dilation, R, was then applied on the previous overlaid image.

$$\mathrm{OP}_3(x) = R_{f_I}(\mathrm{OP}_2) \tag{2}$$

The dilations of marker image (OP_2) under mask image (f_I) were repeated until the contour of marker image fits under the mask image. The reconstructed image is shown in Fig. 3(d). The difference between the original image and the reconstructed image was thresholded at grey level α_2 using the following equation. The value of α_2 is different from image to image depending on automated selection using the Otsu algorithm.

$$\mathrm{OP}_4 = T_{\alpha_2}(f_I - \mathrm{OP}_3) \tag{3}$$

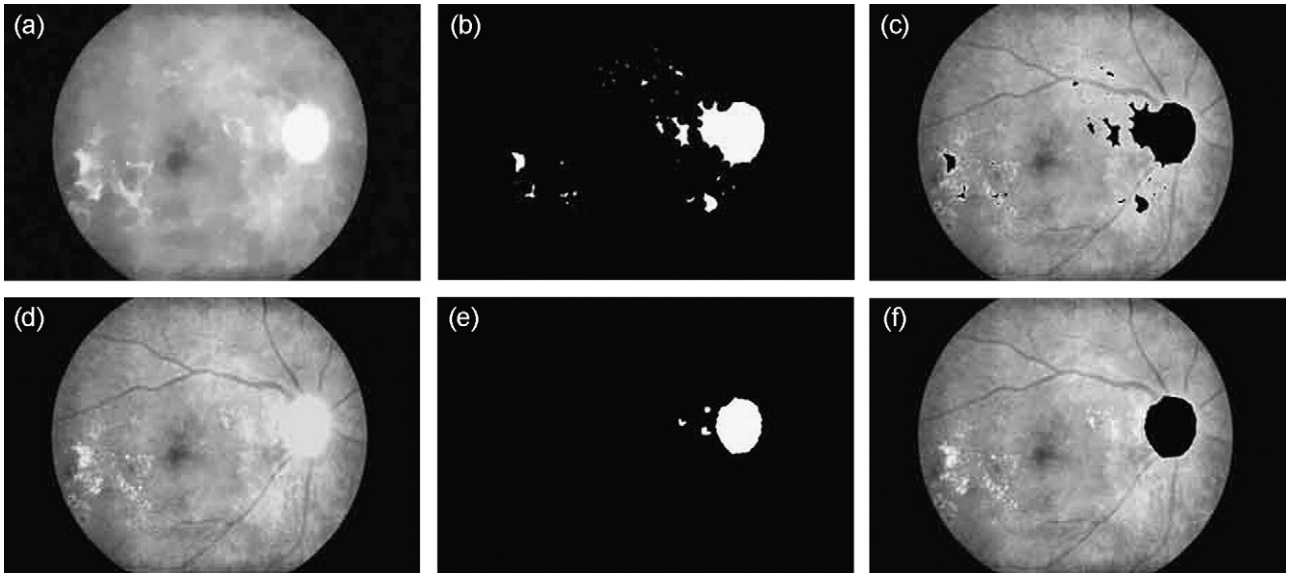

Fig. 3. (a) Intensity image after closing, (b) thresholded image, (c) marker image, (d) reconstructed image, (e) thresholded result of difference image and (f) optic disc area eliminated from the contrast enhanced image.

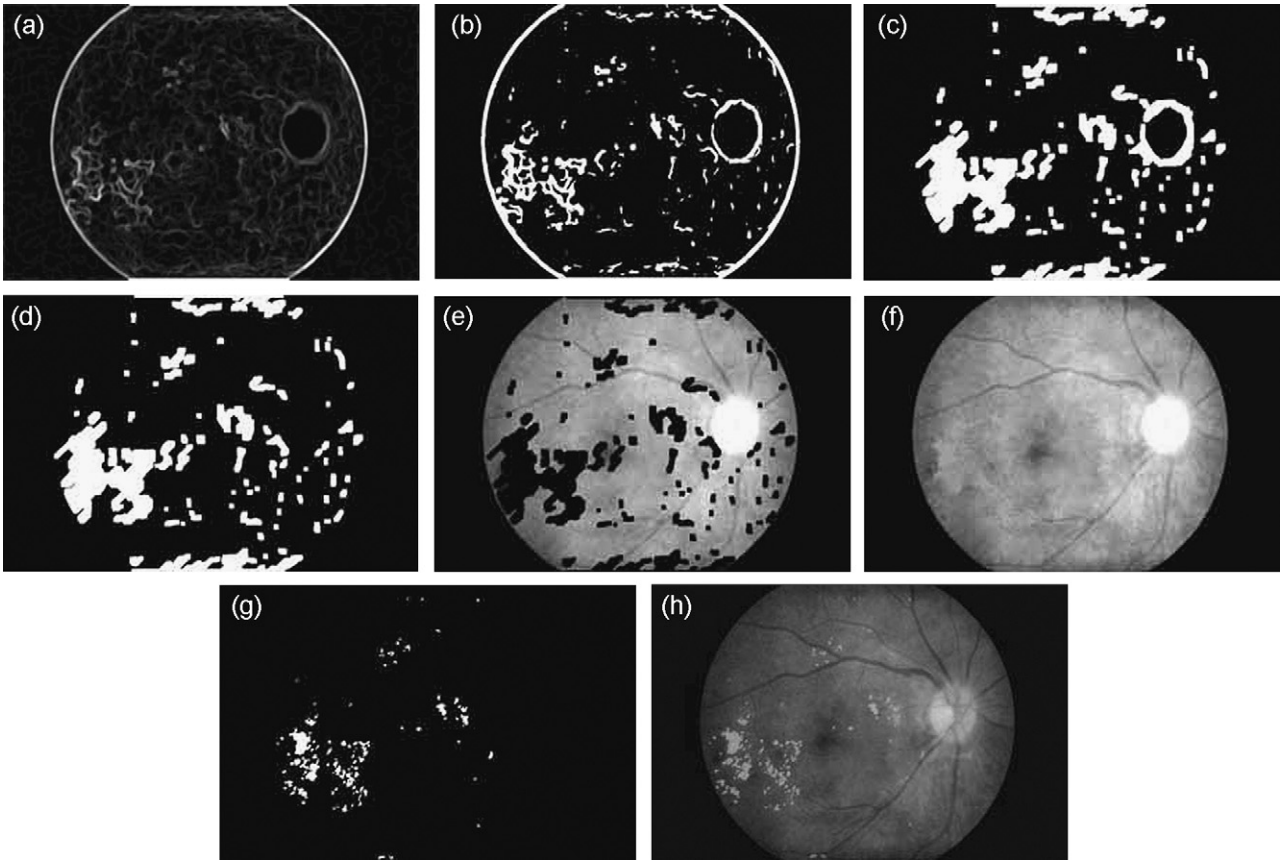

Fig. 4. Exudates detection of "image 1". (a) Local variation image, (b) thresholded image, (c) enclosed areas were flood-filled, (d) optic disc was removed from image, (e) marker image, (f) reconstructed image, (g) difference image AND (h) result superimposed on the original image.

As a result, high intensities are reconstructed while the rest is removed, as shown in Fig. 3(e).

Normally, the optic disc can be easily identified as the largest area. However, in some cases such as the appearance of huge exudates in the image, there might be some areas in the image which are larger than the optic disc. Because the shape of optic disc is round, therefore the optic disc region selection process needs to be made specific to the largest one among the regions whose shapes are circular. Circularity of the shape of the region is defined by the value of compactness, M, as defined using the following equation:

$$M = 4\pi \frac{\text{area}}{\text{perimeter}^2} \tag{4}$$

where area is the number of pixels in the region and perimeter is the total number of pixels around the boundary of each region.

The selected result (largest among circular shapes), OP_5, was dilated with a binary dilation operator (δ) in Eq. (5) to ensure that all pixels in the optic disc area are covered. This step, a flat disc-shaped structuring element with a fixed radius of six (B_2) is used.

$$\text{OP}_{\text{seg}} = \delta^{(B_2)}(\text{OP}_5) \tag{5}$$

All optic disc area in the original image was masked out using the previous output. The result is shown in Fig. 3(f).

2.3. Exudate detection

Similar to the previous steps, high contrast vessels can be eliminated first by a closing operator and it is represented by E_1 in our Eq. (6). A local variation operator, Eq. (6), was then applied to the previous result to get a standard deviation image which shows the main characterization of the closely distributed cluster of exudates. The resulting image, E_2, is shown in Fig. 4(a).

$$E_2(x) = \frac{1}{N-1} \cdot \sum_{i \in W(x)} (E_1(i) - \mu_{E_1}(x))^2 \tag{6}$$

where x is a set of all pixels in a sub-window $W(x)$, N is a number of pixels in $W(x)$, $\mu_{E_1}(x)$ is the mean value of $E_1(i)$ and $i \in W(x)$. A window size of 7×7 was used in this step.

In this step, the resulting image was thresholded at automatically selected grey levels α_3, using the Otsu algorithm, to get rid of all regions with low local variation. To ensure that all the neighbouring pixels of the thresholded result were also included in the candidate region, a binary dilation operator was also applied with a flat disc-shaped structuring element with a fixed radius of six (B_3), as indicated in Eq. (7). The result is shown in Fig. 4(b).

$$E_3 = \delta^{(B_3)}(T_{\alpha_3}(E_2)) \tag{7}$$

The candidate region to represent exudates should not be only their borders, therefore the enclosed area was flood-filled. The image is represented by E_4, and the result is shown in Fig. 4(c). The previously detected optic disc region was dilated before it was used to remove the optic disc from the above resulting flood-filled image (E_4), Eq. (8), the result, E_5, is shown in Fig. 4(d). To implement this step, a binary dilation operator with a flat disc-shaped structuring element with a fixed radius of 10 (B_4) is applied.

$$E_5 = E_4 - \delta^{(B_4)}(\mathrm{OP}_{\mathrm{seg}}) \tag{8}$$

The result from Eq. (8) was used as a mask, showing all possible candidate regions of exudates, to create a marker image (E_6), as shown in Fig. 4(e). It was later morphologically reconstructed using a dilation operator upon the original intensity image similar to the step performed with the detection of the optic disc. The result is displayed in Fig. 4(f).

Using Eq. (9), the final result is obtained by applying a threshold operation at selected grey level α_4 to the difference between the original image (f_{I}) and the reconstructed image (E_7). The resulting image is shown in Fig. 4(g).

$$E_{\mathrm{seg}} = T_{\alpha_4}(f_{\mathrm{I}} - E_7) \tag{9}$$

The result from this step will be sent for validation. Fig. 4(h) displays the thresholded result superimposed on the original image.

There are many parameters used in this experiment. They are, namely, the size of structuring element (B_1, B_2, B_3 and B_4) used for the dilation operation, window size in local variation operator, threshold values (α_1, α_2, α_3 and α_4). α_2 and α_3 were calculated automatically using the Otsu algorithm. B_1, B_2, B_3, B_4, window size, α_1 and α_4 were varied and tested in order to assess the algorithm performance in a previous experiment. Each parameter was varied as follows:

$B_1 \in \{6, 7, 8, 9, 10\}$
$B_2 \in \{4, 5, 6, 7, 8\}$
$B_3 \in \{4, 5, 6, 7, 8\}$
$B_4 \in \{8, 9, 10, 11, 12\}$
window size $\in \{5, 7, 9\}$
$\alpha_1 \in \{0.5, 0.6, 0.7, 0.8, 0.9\}$
$\alpha_4 \in \{0.01, 0.02, 0.03, 0.04, 0.05\}$

From the experiment with different parameter settings, we found that changing the structuring element size and threshold values did not significantly affect the performance of the system. All parameters in this proposed methods are set using the values that gave highest sensitivity and specificity in the previous experiment.

2.4. Macular detection

The macular is detected from the intensity image by the darkest region on the retinal image; it is not always the case due to high illumination. The typical characteristics of the macular (for example, it is within the neighbourhood of the optic disc) is also used to detect the macular more accurately.

The high contrast vessels were eliminated first by a closing operator. The resulting image was binarized by thresholding. Then the darkest area in the neighbourhood of the optic disc (approximately 2.5 times the diameter of the optic disc from the centre of optic disc) was considered as a macular. A Macular grid was drawn according to the ETDRS report [12] with a radius of one third of the optic disc diameter, one optic disc diameter and two optic disc diameters, respectively.

3. Results

Sixty images were tested on an AMD Athlon 1.25 GHz PC using MATLAB. Each image took approximately 3 min to process included the optic disc removal step which took around 1 min. The result of the exudates detection was superimposed on the original image. The previously unclear exudate regions were visibly highlighted and the exudates can be visibly observed after the process. This type of presentation will enable clinicians to identify pathology more quickly. The optic disc was also detected well and removed. Usually there are no exudate pixels around the optic disc so the removal of the optic disc did not affect the exudate detection. An example of the detection results are shown in Fig. 5.

The performance of our technique was evaluated quantitatively by comparing the resulting extractions with ophthalmologists' hand-drawn ground-truth images pixel by pixel. In order to facilitate the experts to produce a ground-truth image, a first draft of ground-truth image was created by us. We marked the very obvious exudate pixels which are normally bright and yellowish areas, pixel by pixel, using a photo manipulation program with one colour. Then, this first draft image was shown to two expert ophthalmologists together with the original image. The ophthalmologists then made some changes by adding some missing exudate pixels and/or removing some misunderstood non-exudate pixels until it was agreed by both experts.

Sensitivity and specificity were chosen as our measurement of accuracy of the algorithms at the pixel level. Not only does this evaluation mechanism show how accurate our detection was, it also shows how inaccurate our detector can be. This pixel-based evaluation considers four values, namely true positive (TP), a number of exudates pixels correctly detected, false positive (FP), a number of non-exudate pixels which are detected wrongly as exudate pixels, false negative (FN), a number of exudate pixels that were not detected and true negative (TN), a number of non-exudates pixels which were correctly identified as non-exudate pixels. From these quantities, the sensitivity and specificity were computed using Eqs. (10) and (11). The misclassified proportion was computed using Eq. (12).

$$\text{sensitivity} = \frac{\mathrm{TP}}{\mathrm{TP} + \mathrm{FN}} \tag{10}$$

$$\text{specificity} = \frac{\mathrm{TN}}{\mathrm{TN} + \mathrm{FP}} \tag{11}$$

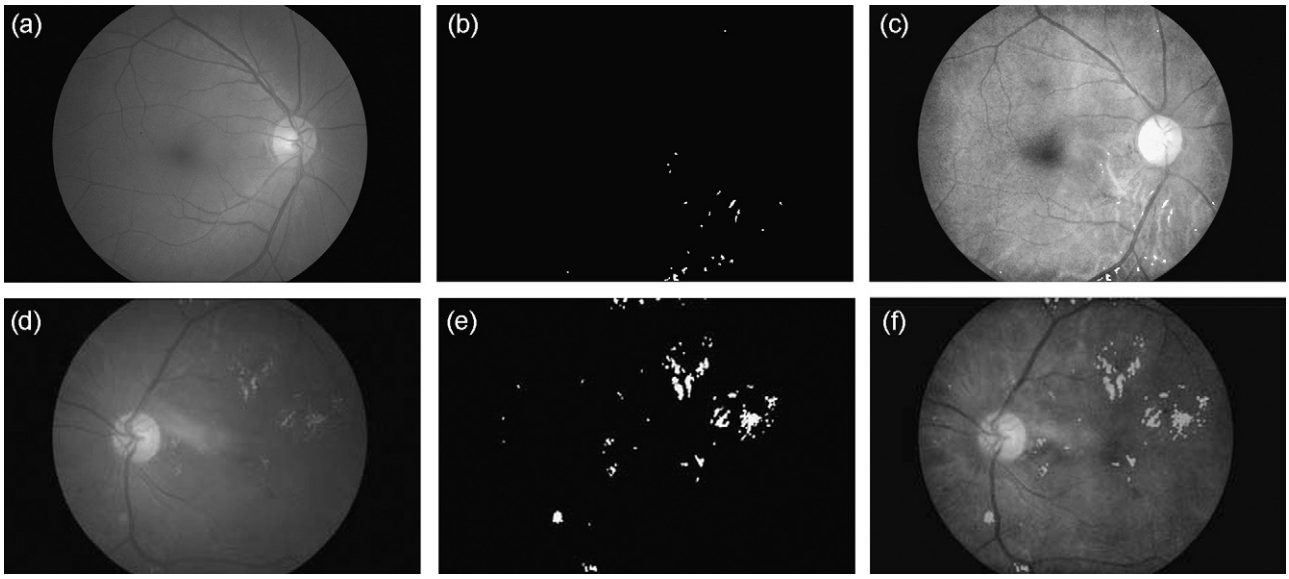

Fig. 5. Exudates detection on low contrast images. (a) Original images of a normal eye, (b) detected structures (exudate-like) of (a), (c) detected structures superimposed on contrast enhanced images, (d) original images of a diseased eye, (e) detected exudates of (d), and (f) detected exudates superimposed on contrast enhanced images.

$$\text{misclassified proportion} = \frac{\text{FP}}{\text{TP} + \text{FP} + \text{FN} + \text{TN}} \tag{12}$$

After all the 40 retinal images with exudates and 20 normal retinal images without exudates were processed, they were compared with the hand-drawn ground-truth images. Table 1 shows the quantitative result of TP, FP, FN, TN, sensitivity, specificity and misclassified proportion from the images of diseased eyes. For our data set with diabetic retinopathy exudates, the sensitivity and specificity of the exudate detection are 80% and 99.5%, respectively. For normal retinal image detection, the specificity and misclassified proportion are 99.9% and 7.2%, respectively. The sensitivity cannot be calculated in which TP and FN values are all zero due to no exudates in ground-truth images.

Our algorithm has very high specificity which showed that the algorithm does not recognize a non-exudate pixel as an exudate pixel. However, the sensitivity, a relatively lower value, also showed that the low intensity exudates pixels are still too elusive to be detected by this algorithm.

The system also detects the macular region in order to provide the ophthalmologists with the distance information between the detected exudates and the macular. The exudates within the inner circle will affect the vision of patients more than the ones outside it. As shown in Fig. 6(a), exudates are present nearer to the macular than exudates in Fig. 6(b). This indicates that the exudates in Fig. 6(a) will be more harmful to vision than those in Fig. 6(b).

4. Discussion

In this work we have investigated and proposed a set of optimally adjusted morphological steps to automatically detect optic disc and exudates from diabetic retinopathy patient's non-dilated pupil digital images in an attempt to detect the pathologies earlier. The optic disc was detected and removed prior to the exudate detection because the intensity features of both areas are similar.

From 20 normal patients, the misclassified proportion value of seven people is over the average misclassified proportion and might need a further diagnosis. It means that this system can reduce the ophthalmologist's workload especially in developing countries where the number of ophthalmologists is not sufficient to deal with the large number of diabetic retinopathy patients.

This system intends to help the ophthalmologists in the diabetic retinopathy screening process for detecting the symptoms faster and more easily. The results demonstrated here indicate that automated diagnosis of diabetic retinopathy based on intensity retinal image analysis can be very successful in detecting exudates. It is not a final result application but it can be a preliminary diagnosis tool or decision support system for oph-

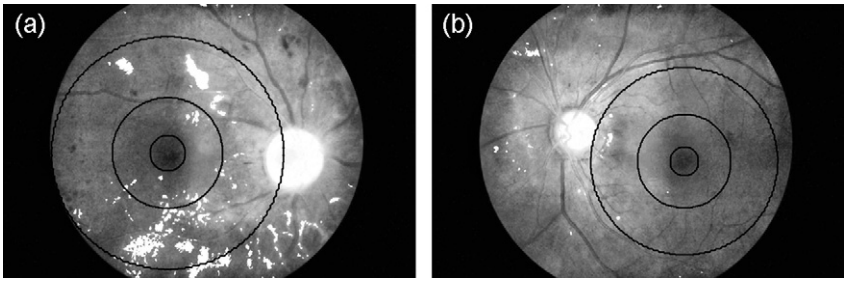

Fig. 6. (a) and (b) Macular grid centred on the macular, superimposed on the exudate detection result.

Table 1
The exudates detection results of diseased retinal images

24-Bit images	Ground-truth exudates numbers	Detected exudates numbers	TP	FP	FN	TN	Sensitivity (%)	Specificity (%)	Misclassified proportion (%)
Image 1	9,215	10,431	6,575	3,856	2,640	362,929	71.35	98.95	102.55
Image 2	1,172	1,397	958	439	214	374,389	81.74	99.88	11.68
Image 3	410	762	261	501	149	375,089	63.66	99.87	13.32
Image 4	307	1,049	188	861	119	374,832	61.24	99.77	22.90
Image 5	1,453	1,903	1,150	753	303	373,794	79.15	99.80	20.03
Image 6	1,241	2,498	1,083	1,415	158	373,344	87.27	99.62	37.63
Image 7	1,879	2,993	1,600	1,393	279	372,728	85.15	99.63	37.05
Image 8	262	1,038	154	884	108	374,854	58.78	99.76	23.51
Image 9	2,043	3,103	1,653	1,450	390	372,507	80.91	99.61	38.56
Image 10	519	841	425	416	94	375,065	81.89	99.89	11.06
Image 11	642	1,284	521	763	121	374,595	81.15	99.80	20.29
Image 12	144	911	112	799	32	375,057	77.78	99.79	21.25
Image 13	1,257	1,789	871	918	386	373,825	69.29	99.76	24.41
Image 14	659	1,360	379	981	280	374,360	57.51	99.74	26.09
Image 15	10,670	12,115	8,782	3,333	1,888	361,997	82.31	99.09	88.64
Image 16	721	1,392	716	676	5	374,603	99.31	99.82	17.98
Image 17	1,233	1,881	998	883	235	373,884	80.94	99.76	23.48
Image 18	494	762	337	425	157	375,081	68.22	99.89	11.30
Image 19	432	1,049	258	791	174	374,777	59.72	99.79	21.04
Image 20	109	480	75	405	34	375,486	68.81	99.89	10.77
Image 21	3,683	5,281	2,865	2,416	818	369,901	77.79	99.35	64.26
Image 22	15,557	17,446	12,780	4,666	2,777	355,777	82.15	98.71	124.10
Image 23	4,016	5,098	3,271	1,827	745	370,157	81.45	99.51	48.59
Image 24	3,375	4,638	2,745	1,893	630	370,732	81.33	99.49	50.35
Image 25	7,774	10,431	6,340	4,091	1,434	364,135	81.55	98.89	108.80
Image 26	1,132	1,397	956	441	176	374,427	84.45	99.88	11.73
Image 27	3,602	5,151	2,932	2,219	670	370,179	81.40	99.40	59.02
Image 28	526	1,531	435	1,096	91	374,378	82.70	99.71	29.15
Image 29	26,135	32,401	24,279	8,122	1,856	341,743	92.90	97.68	216.01
Image 30	38,302	41,456	34,845	6,611	3,457	331,087	90.97	98.04	175.82
Image 31	7,700	11,293	6,880	4,413	820	363,887	89.35	98.80	117.37
Image 32	17,882	20,026	16,352	3,674	1,530	354,444	91.44	98.97	97.71
Image 33	3,451	5,417	2,720	2,697	731	369,852	78.82	99.28	71.73
Image 34	4,063	6,127	3,426	2,701	637	369,236	84.32	99.27	71.84
Image 35	9,151	9,609	7,713	1,896	1,438	364,953	84.29	99.48	50.43
Image 36	2,286	3,325	2,162	1,163	124	372,551	94.58	99.69	30.93
Image 37	11,003	12,974	10,188	2,786	815	362,211	92.59	99.24	74.10
Image 38	3,211	3,801	2,590	1,211	621	371,578	80.66	99.68	32.21
Image 39	458	1,435	379	1,056	79	374,486	82.75	99.72	28.09
Image 40	850	2,573	752	1,821	98	373,329	88.47	99.51	48.43
Average							80.00	99.46	52.36

thalmologists. Human ophthalmologists are still needed for the cases where detection results are not very obvious.

It is suggested by Javitt et al. [19] that a system with a sensitivity of 60% or greater maximized cost effectiveness using for diabetic retinopathy screening, the result from our system is well above that.

There are also some incorrect exudate detections which are caused by the artefacts that are similar to exudates, artefacts from the noise in the image acquisition process, the exudates that are proximate to blood vessels or because the exudates appear very faint. There are also some incorrect exudate-like detections on a normal retinal image as shown in Fig. 5(b). Strong and high contrast choroidal blood vessels, which appear and lie in the retina background are incorrectly detected as exudates. The missing faint exudates may have not affected the sensitivity much since even human experts are not sure about some ambiguous regions. However, the performance of the algorithm can be improved if these set of low-contrast exudates can be detected. We might have to add more specific features to the system in order to get these kinds of regions to be detected in the future.

One main weakness of the algorithm arises from the fact that the algorithm depends on other tasks, namely, the detection of the optic disc, and vessel removal. The results of exudate detection depend on the success of these methods. This indicates the further necessity of improving the robustness of these tasks.

5. Conclusion and future work

This method was developed to detect exudates from non-mydriatic, low-contrast, retinal digital images of retinopathy patients and it is intended to help the ophthalmologists in the diabetic retinopathy screening process to detect symptoms faster and more easily. The proposed techniques work effectively even on a poor computing system.

The results also provide ophthalmologists with distance information between the detected exudates and the macular. The retinal vessel detection could also be added in order to facilitate ophthalmologist decisions on laser treatment. The results of this work can be developed to produce an automated system to detect exudates. Microaneurysm and haemorrhage detection could be added to the system in order to increase its ability to verify the degree of diabetic retinopathy. It will be useful to extend this work by developing a system to detect them.

Future work will address an issue of improving the sensitivity by improving the results of other tasks, such as the detection of the optic disc and blood vessels, and also try to localize faint and small exudates. In future, in work to expand the detection system to recognize microaneurysms and haemorrhages, there may be a problem in separating the pathologies from small vessels. We can detect vessels prior to the detection of pathologies and subtract them from the image. If small vessels are missed during this step and are confused with microaneurysms or haemorrhages it may be possible to combine more than one detection technique [5] to make a final decision on the likelihood of the detected area being either a vessel or microaneurysm or a haemorrhage.At the moment our algorithm is not able to detect differences between hard and soft exudates. However, hard and soft exudates can be distinguished by their colour and the sharpness of their border so this could be detected by tuning the edge filter and feature selection. It is intended that these features will be used in future detection algorithms.

Additionally, ground-truth creation may also be done solely by expert ophthalmologists in order to reduce authors' bias and the results from that test set may be used to compare with the current one.

Acknowledgement

We would like to thank Eye Care Centre, Thammasat University Hospital who supplied all the images used in this project for its great support for the project.

References

[1] Ege BM, Hejlesen OK, Larsen OV, Moller K, Jenning B, Kerr D. Screening for diabetic retinopathy using computer based image analysis and statistical classification. Comput Methods Prog Biomed 2000;62:165–75.
[2] Hove MN, Kristensen JK, Lauritzen T, Bek T. Quantitative analysis of retinopathy in type 2 diabetes: dentification of prognostic parameters for developing visual loss secondary to diabetic maculopathy. Acta Ophthalmol Scand 2004;82:679–85.
[3] Hsu W, Pallawala PMDS, Mong Li Lee, Kah-Guan Au Eong. The role of domain knowledge in the detection of retinal hard exudates. In: Proceedings of the International Conference on Computer Vision and Pattern Recognition IEEE Computer Society, vol. 2. 2001. p. II-246–51.
[4] Kanski J. Diabetic retinopathy, clinical ophthalmology. Oxford: Butterworth-Heimann; 1997.
[5] Sinthanayothin C, Boyce JF, Williamson TH, Cook HL, Mensah E, Lal S. Automated detection of diabetic retinopathy on digital fundus image. J Diabet Med 2002;19:105–12.
[6] Niemeijer M, van Ginneken B, Staal J, Suttorp-Schulten MS, Abramoff MD. Automatic detection of red lesions in digital color fundus photographs. IEEE Trans Med Imag 2005;24:584–92.
[7] Usher D, Dumskyj M, Himaga M, Williamson TH, Nussey S, Boyce J. Automated detection of diabetic retinopathy in digital retinal images: a tool for diabetic retinopathy screening. Diabet Med 2004;21:84–90.
[8] Gardner GG, Keating D, Williamson TH, Elliott AT. Automatic detection of diabetic retinopathy using an artificial neural network: a screening tool. Br J Ophthalmol 1996;80:940–4.
[9] Zheng Liu, Opas C, Krishnan SM. Automatic image analysis of fundus photograph. In: Proceedings of the International Conference on Engineering in Medicine and Biology, vol. 2. 1997. p. 524–5.
[10] Osareh A, Mirmehdi M, Thomas B, Markham R. Automated identification of diabetic retinal exudates in digital colour images. Br J Ophthalmol 2003;87:1220–3.
[11] Mitra SK, Te-Won Lee, Goldbaum M. Bayesian network based sequential inference for diagnosis of diseases from retinal images. Pattern Recogn Lett 2005;26:459–70.
[12] ETDRS Report Number 10, Grading diabetic retinopathy from stereoscopic color fundus photographs—an extension of the modified Airlie house classification. Ophthalmology 1991;98:786–806.
[13] Davis MD, Bressler SB, Aiello LP, Bressler NM, Browning DJ, Flaxel CJ, et al. Comparison of time-domain oct and fundus photographic assessments of retinal thickening in eyes with diabetic macular edema. Invest Ophthalmol Vis Sci 2008;49:1745–52.
[14] Gonzales RC, Woods RE. Digital image processing. New York: Addison-Wesley; 1993. p. 75–140.
[15] Sinthanayothin C, Boyce JF, Cook HL, Williamson TH. Automated localization of the optic disc, fovea, and retinal blood vessels from digital colour fundus images. Br J Ophthalmol 1999;83:902–10.
[16] Walter T, Klein JC, Massin P, Erginay A. A Contribution of image processing to the diagnosis of diabetic retinopathy—detection of exudates in colour fundus images of the human retina. IEEE Trans Med Imag 2002;21:1236–43.
[17] Sanchez CI, Hornero R, Lopez MI. Retinal image analysis to detect and quantify lesions associated with diabetic retinopathy. In: Proceedings of the International Conference on Engineering in Medicine and Biology Society IEEE. 2004. p. 1624–7.
[18] Zhang X, Opas C. Detection and classification of bright lesions in colour fundus images. In: Proceedings of the International Conference on Image Processing IEEE. 2004. p. 139–42.
[19] Javitt JC, Aiello LP, Bassi LJ, Chiang EP, Canner JK, Klein R. Detecting and treating retinopathy in patients with type I diabetes mellitus. Savings associated with improved implementation of current guidelines. Ophthalmology 1991;98:1565–73.

Akara Sopharak received the B.Sc. and M.Sc. degrees in Computer Science from Burapha University and Mahidol University, Thailand, in 1998 and 2002, respectively. She is currently a doctor degree student at Sirindhorn International Institute of Technology, Thammasat University. Her research interests include medical image processing.

Bunyarit Uyyanonvara is currently an assistant professor in Information Technology at Sirindhorn International Institute of Technology, Thammasat University. He received his B.Sc. (1st Class Honors) in Science from Prince of Songkhla University, in 1995 and his Ph.D. in Medical Image Processing from King's College, University of London, in 2000.

Sarah Barman qualifications include a B.Sc. in physics from Essex University, an M.Sc. in applied optics from Imperial College, University of London and a Ph.D. in optical physics from King's College, University of London. Since 2000, Dr. Barman has been based at the Digital Imaging Research Centre at Kingston University and is currently investigating medical imaging algorithms, based on her experience of image processing and optical modeling techniques for use on a range of ophthalmic images.

Thomas H. Williamson, Consultant Ophthalmologist and Vitreoretinal Specialist in London, UK. He is a senior consultant Ophthalmologist at St. Thomas' Hospital, London, Queen Mary's Hospital, Sidcup, Kent, and an Honorary Clinical Lecturer at King's College, London. His specialist area of interest is retinal disease and surgery. He also has an over 20 years experience in the care of the eye and 13 years as a vitreoretinal specialist.